ISSN 1054-660X, Laser Physics, 2007, Vol. 17, No. 4, pp. 358–367.

Single and Double Ionization of the Hydrogen Molecule in an Intense Few-Cycle Laser Pulse

S. Baier[a, *], C. Ruiz[a], L. Plaja[b], and A. Becker[a, **]

[a] *Max-Planck-Institut für Physik komplexer Systeme, Nöthnitzer Str. 38, Dresden, D-01187 Germany*
[b] *Departemento de Fisica Aplicada, Universidad de Salamanca, Salamanca, E-37008 Spain*

*e-mail: silvio@mpipks-dresden.mpg.de
**e-mail: abecker@mpipks-dresden.mpg.de

Received October 27, 2006

Abstract—In this paper, we present ab initio two-electron model calculations of laser-induced single and double ionization of the hydrogen molecule in a linearly polarized laser field with static nuclei located along the polarization axis. Within the model, the center-of-mass motion of the two electrons is restricted along the polarization axis of the field, while the relative electron motion is unrestricted. The results of numerical simulations allow us to identify and characterize the mechanisms leading to single and double ionization in an intense few-cycle laser pulse. The role of the rescattering mechanism on the ionization processes is analyzed in particular.

PACS numbers: 33.80.Rv, 32.80.Rm, 42.50.Hz

DOI: 10.1134/S1054660X07040111

1. INTRODUCTION

Since the availability of ultrashort intense laser pulses the experimental and theoretical research of laser-induced processes in atoms and molecules is a permanently growing field. To control the electron and nuclear dynamics induced by an intense laser pulse it is important to first analyze the pathways to ionization, dissociation and fragmentation of a molecule (for a review, see, e.g., [1]). In this respect the hydrogen molecule, which is one of the simplest molecules and easily accessible for experimental studies, has drawn the attention of many groups. Different phenomena in strong laser fields such as dissociation [2–4], charge resonance enhanced ionization of the H_2^+ ion [5–7], sequential [8, 9] and nonsequential double ionization [8, 10, 11] have been observed. Note, that many of these processes, such as sequential double ionization and charge resonance enhanced ionization, are effective one-electron processes, where either only one electron or both electrons independently interact with the field and the electron–electron interaction is negligible.

In contrast, nonsequential double ionization is an elementary example of a correlated two-electron process, in which electron–electron interaction plays an important role. In atoms, the main mechanism leading to the joint emission of two electrons in a near-infrared laser pulse has been identified as the so-called rescattering scenario [12–19]. According to this picture, first one of the electrons is emitted via the interaction with the linearly polarized field, then it is accelerated and driven back to the parent ion by the field, where it interacts with the residual electron via the electron correlation interaction. As a result, either both electrons instantaneously leave the atom together or the second electron is excited and then emitted from the excited state at a subsequent maximum of the field [12, 20, 21]. Recent experiments [22] and simulations [23] show that these basic mechanisms appear to be similar in molecules, too.

Ab initio simulations of the Schrödinger equation of the hydrogen molecule interacting with an intense external laser field, even in the case of fixed nuclei, requires the solution of a differential equation with six dimensions in space and one in time. In case of linear polarization of the field and an aligned orientation of the molecule, where the nuclei are fixed along the field polarization axis, the dimensionality of the problem is reduced by one due to the symmetry in the geometry. An ab initio solution of the corresponding equation at high intensities and low frequencies of the laser pulse is, however, still at the limit of current high-power supercomputers. In order to reduce the computational effort, so-called one-dimensional models, in which the motion of both electrons is restricted along the polarization axis, are often used [24]. This approximation has been applied successfully to (at least qualitatively) analyze effective one-electron effects in linearly polarized fields, e.g., single ionization, charge resonant enhanced ionization or sequential double ionization, in which the highly nonlinear electron-laser interaction directed along the polarization direction is the main source of the dynamics. However, it is arguable whether this approximation should still lead to useful results if other interactions besides the nonlinear field interaction become relevant for the process of interest. As outlined above, the nonsequential double ionization is a such an example, where the electron–electron interaction plays a dominant role at infrared wavelengths, too. Since the electron correlation interaction, $1/r_{12}$,

does not have the same preferred directionality as the electron–field interaction, the one-dimensional model can generate results which are not even qualitatively in agreement with the experimental observations of nonsequential double ionization [25]. As an alternative, we have recently introduced a two-electron approach in which the center-of-mass motion of the two electrons, which is coupled to the laser field, is restricted along the field direction, while the relative electron motion which couples to the electron–electron interaction is kept unchanged [12, 23]. Our first numerical results have revealed a strong electron dynamics perpendicular to the laser axis due to the Coulomb correlation between the electrons.

In this paper, we use the model to present a detailed analysis of two-electrons effects in single and double ionization of the hydrogen molecule interacting with a few-cycle intense laser pulse. The paper is organized as follows: in Section 2, we introduce and discuss the two-electron model. Next, in Section 3 we present results of numerical simulations for the total yields of single and double ionization and the electron distributions at different time instants during the pulse. Then we will identify and characterize the dominant pathways to single and double ionization of the two-electron molecule. Finally, we will analyze the recollision mechanism by comparing numerical results obtained on grids of different spatial size with each other. The conclusions are given in Section 4.

2. TWO-ELECTRON MODEL

The two-electron Hamiltonian for a hydrogen molecule with static nuclei interacting with an intense laser pulse, linearly polarized along the z direction, can be written as (Hartree atomic units, $e = m = \hbar = 1$, are used):

$$H = \frac{\mathbf{P}^2}{4} + \mathbf{p}^2 - \frac{\mathbf{P}\cdot\mathbf{A}(t)}{c} + \frac{1}{r} - \frac{2}{|2\mathbf{R}+\mathbf{R}_k+\mathbf{r}|} - \frac{2}{|2\mathbf{R}+\mathbf{R}_k-\mathbf{r}|} - \frac{2}{|2\mathbf{R}-\mathbf{R}_k+\mathbf{r}|} - \frac{2}{|2\mathbf{R}-\mathbf{R}_k-\mathbf{r}|}, \quad (1)$$

where $\mathbf{R} = (\mathbf{r}_1 + \mathbf{r}_2)/2$, $\mathbf{P} = \mathbf{p}_1 + \mathbf{p}_2$, $\mathbf{r} = \mathbf{r}_1 - \mathbf{r}_2$, and $\mathbf{p} = (\mathbf{p}_1 - \mathbf{p}_2)/2$ are the center-of-mass and relative coordinates and momenta of the two electrons, respectively. $\pm\mathbf{R}_k/2$ denote the positions of the two nuclei, where the origin of the coordinate system is set to be in the middle between the nuclei, and $\mathbf{A}(t)$ is the vector potential of the linearly polarized field.

It is important to note that, in the above form of the Hamiltonian, the two most relevant interactions for the joint nonsequential double electron emission, namely, the electron–field interaction term and the electron–electron Coulomb interaction term, are decoupled in the center-of-mass coordinate on the one and in the relative coordinate on the other hand. This allows us to reduce the dimensionality of the Hamiltonian by restricting the center-of-mass motion along the polarization axis ϵ without changing the electron–electron interaction term. For σ states of the H_2 molecule with nuclei located along the polarization axis, the Hamiltonian is symmetric in the relative coordinate over rotation about the polarization axis. Thus, we can write the two-electron model Hamiltonian in cylindrical coordinates (ρ, z, Z) as

$$H = \frac{P_z^2}{4} + p_\rho^2 + p_z^2 - \frac{P_z A(t)}{c} + \frac{1}{\sqrt{\rho^2+z^2}} - \frac{1}{\sqrt{\left(Z+\frac{z}{2}+\frac{R_k}{2}\right)^2+\frac{\rho^2}{4}+a^2}} - \frac{1}{\sqrt{\left(Z-\frac{z}{2}+\frac{R_k}{2}\right)^2+\frac{\rho^2}{4}+a^2}} - \frac{1}{\sqrt{\left(Z+\frac{z}{2}-\frac{R_k}{2}\right)^2+\frac{\rho^2}{4}+a^2}} - \frac{1}{\sqrt{\left(Z-\frac{z}{2}-\frac{R_k}{2}\right)^2+\frac{\rho^2}{4}+a^2}}, \quad (2)$$

where a parameter a^2 is introduced to soften the attractive Coulomb potentials in the numerical calculations. The coordinates are illustrated in Fig. 1. Z denotes the center-of-mass motion of the two electrons, which is restricted to the polarization direction, z and ρ represent the relative coordinates of the two electrons parallel and perpendicular with respect to the polarization axis.

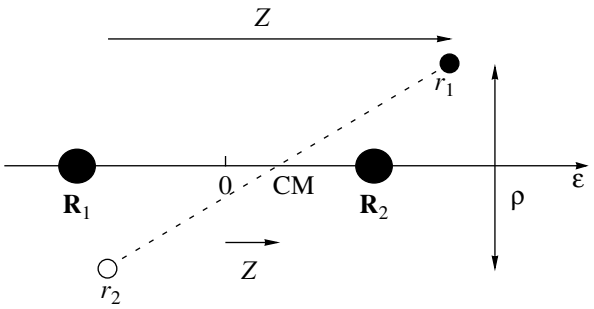

Fig. 1. Illustration of the coordinate system: $\mathbf{R}_1$ and $\mathbf{R}_2$ denote the positions of the nuclei located symmetric about the center of the coordinate system along the polarization axis, ϵ, while $\mathbf{r}_1$ and $\mathbf{r}_2$ denote the positions of the electrons. Cylinder coordinates (z, ρ) for the relative coordinate $\mathbf{r}$ are used. The center-of-mass motion of the two-electron system (Z) is restricted along the polarization axis.

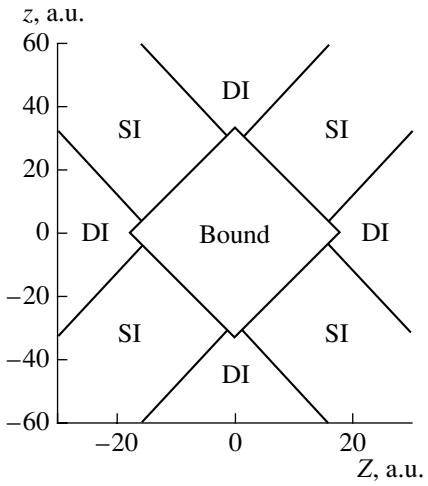

Fig. 2. Single ionization (SI = H_2^+) and double ionization (DI = H_2^{2+}) are defined by different regions in the coordinate space, which are shown for $\rho = 0$.

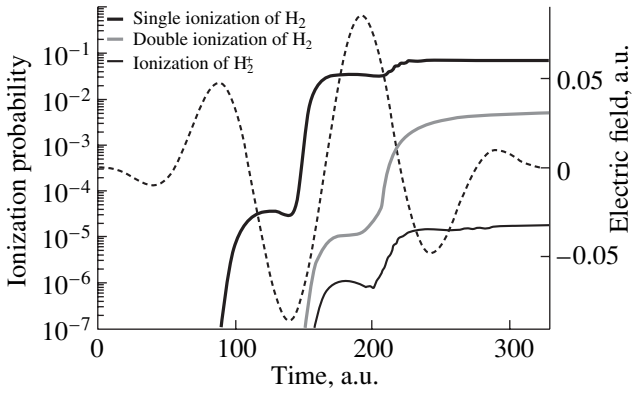

Fig. 3. Single (thick line) and double ionization probabilities (grey line) of H_2 molecule as a function of time. The amplitude of the electric field is displayed by the dashed line. Also shown are the results of test calculations for the single ionization of H_2^+ (thin line), multiplied by the H_2^+ probability.

Please note that, in the above approximation, the coordinates of the two electrons along the polarization axis are independent of each other. However, due to the restriction of the center-of-mass motion along the polarization axis, the coordinates and the motion of the two electrons perpendicular to the axis have to be symmetric. Of course, this introduces a correlation between the electrons which is not present in the unrestricted two-electron Hamiltonian. Before we proceed, we may further note that the model is in the spirit of the original one-dimensional approach of the single-active-electron Hamiltonians [26]. However, it appears to be a more general extension of the 1D approach to many-electron systems than the usual restriction of the motion of each electron independently, since it makes use of the well-known fact that an external field couples to the center-of-mass of a many-body (here, two-electron) system.

The initial state wavefunction is the molecular ground state of H_2 which is obtained via imaginary time propagation. The parameters $R_k = 2.042$ a.u. and $a^2 = 0.415$ are chosen such that the ground state energies of the neutral molecule and its ion are –1.1743 and –0.6235 a.u., respectively. For the actual numerical calculations, we have used a three-cycle laser pulse of the form

$$E(t) = \mathscr{E}_0 \sin^2\left(\frac{\omega t}{6}\right)\sin(\omega t - 3\pi) \qquad (3)$$

with a carrier frequency of $\omega = 0.057$ a.u. (which corresponds to a wavelength $\lambda = 800$ nm) and a peak amplitude of $\mathscr{E}_0 = 0.091$ a.u. (which corresponds to a peak intensity $I_0 = 2.9 \times 10^{14}$ W/cm^2). The Schrödinger equation with the Hamiltonian (2) was solved on a grid with spatial steps $\Delta\rho = \Delta z = \Delta Z = 0.5$ a.u., time step $\Delta t = 0.025$ a.u., and 150 grid points in the ρ direction, 500 in the z direction, and 250 in the Z direction. A $\cos^{1/2}$-like absorbing mask function has been used to avoid reflections at the boundaries. As will be seen below, the grid is chosen large enough to identify and characterize the mechanisms leading to single and nonsequential double ionization of the hydrogen molecule. Please note that other processes such as dissociation and charge resonance enhanced ionization are suppressed due to the choice of fixed nuclei in the calculations. This is justified by recent experimental observations [27, 28] that the nonsequential mechanism is the dominant pathway to double ionization of the H_2 molecule in a few-cycle laser pulse.

In order to analyze the results in view of single and double ionization, we have partitioned the coordinate space as follows:

H_2 molecule: $r_1 < 17.3$ a.u. and $r_2 < 17.3$ a.u.

H_2^+ ion: either $r_1 < 14.0$ a.u. and $r_2 > 17.3$ a.u.

or $r_1 > 17.3$ a.u. and $r_2 < 14.0$ a.u.

H_2^+ ion: complementary space

with $r_1 = \sqrt{\left(Z + \frac{z}{2}\right)^2 + \frac{\rho^2}{4}}$ and $r_2 = \sqrt{\left(Z - \frac{z}{2}\right)^2 + \frac{\rho^2}{4}}$. In Fig. 2, we visualize the different regions for $\rho = 0$. The choice of two different distances in the partition ensures that probability density can transfer directly from the region of the neutral H_2 molecule (bound) to the region of the double ionized H_2^{2+} molecular ion (DI) without passing the region of single ionization (SI). The boundaries are chosen such that the probability densities are decreased by more than 13 orders of magnitude with respect to the maximum of the corresponding bound state.

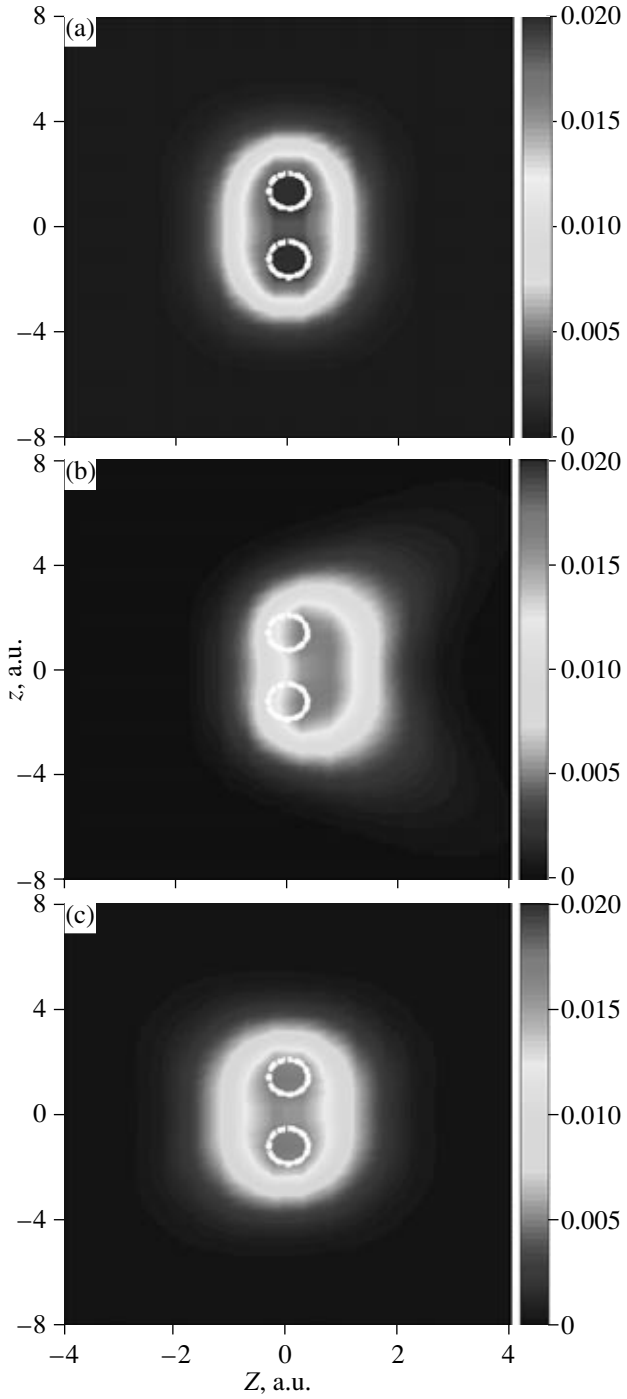

Fig. 4. Z, z-probability density integrated over the perpendicular coordinate ρ three different time instants, namely (a) $t = 0$ (initial ground state), (b) $t = 143$ a.u. (near field maximum) and (c) at $t = 166$ a.u. (at field zero). The dashed white circles represent the positions of the maxima in the ground state distribution.

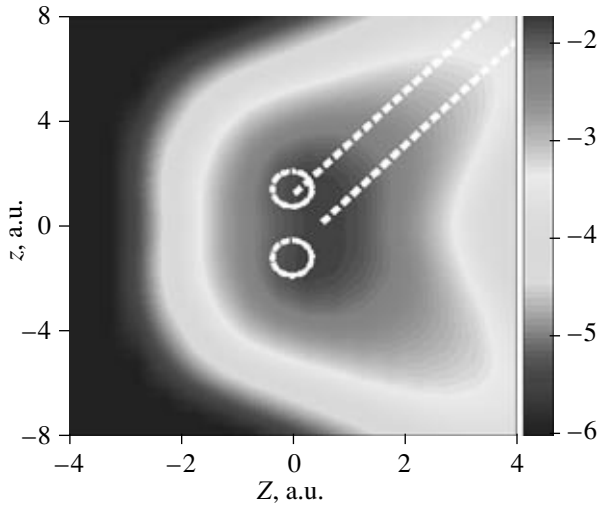

Fig. 5. Same as Fig. 4b) but on a logarithmic scale. The dashed lines show the directions of single ionization expected from the covalent and the ionic part, respectively.

3. RESULTS OF NUMERICAL CALCULATIONS

Figure 3 represents the results of the numerical calculations for the single (thick line) and double ionization (grey line) probabilities along with the amplitude of the electric field (dashed line) as a function of time. As can be seen from the figure, the single ionization probability rises three times just beyond the field maxima as expected from the field (or tunnel) ionization picture. The short delay with respect to the field maxima is caused by the time the singly ionized electron wave packet needs to pass from the bound region to the SI region in the partition of the coordinate space. We note that the single ionization probability slightly decreases (before the second and third steep rise) due to the return of part of the singly ionized wave packet to the residual ion (i.e., the bound region in the coordinate space). The double ionization probability curve shows two steep rises around the zeros of the field, which is in agreement with the expectations of the direct rescattering picture [13]. Please note another small increase near the second field maximum, which is found to correspond to the field ionization of excited ionic states [23]. Indeed, this can be seen by the comparison with the results of test calculations, in which the repulsion term $1/r$ is removed from Eq. (2). The resulting Hamiltonian is equivalent to two independent electrons in the H_2^+ potential of our model. The results shown by the thin line in Fig. 3 are obtained by starting from the ground state of this system, using the same laser pulse and multiplying the ionization probability with the previously obtained H_2^+ single ionization probability (thick line in Fig. 3). As can be seen from the comparison, these test results (thin line) are at least one order of magnitude lower than the double ionization probability (grey line) at any time instant. This shows that the latter does not arise from field ionization of the molecular ions in its ground state. In the next two subsections, we analyze the pathways to single and double ionization in more detail.

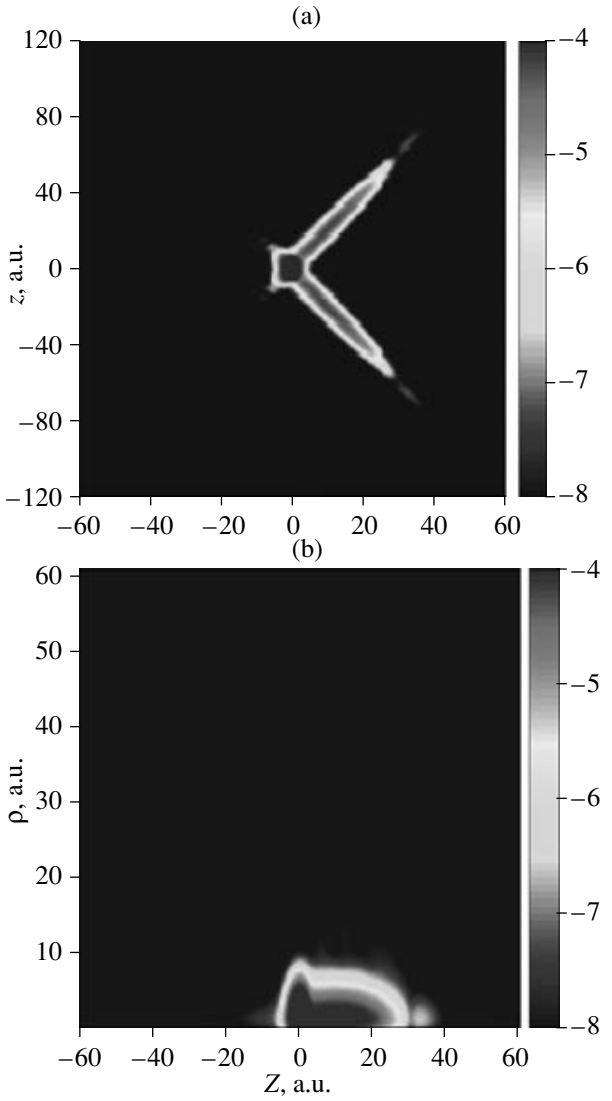

Fig. 6. Probability density distributions integrated over (a) ρ, and (b) z at t = 166 a.u. (zero of the field). It is seen the emission of a singly ionized electron wavepacket along the polarization direction.

3.1. Two-Electron Effects in Single Ionization

We first investigate the effects of correlated electron dynamics in the neutral molecule and on the single ionization pathway. This is motivated by the results of earlier theoretical studies [29, 30] that ionization of the hydrogen molecule in an intense laser field primarily proceeds via ionic doorway states, which are formed at the maxima of the electric field. Our results, shown in Figs. 4 and 5, confirm these findings.

Figure 4 displays snapshots of the probability density (on a linear scale) as a function of Z and z, integrated over the perpendicular component of the relative coordinate, ρ, at three instants of time, namely, (Fig. 4a) t = 0 (initial ground state), (Fig. 4b) t = 143 a.u. (near field maximum), and (Fig. 4c) t = 166 a.u. (at field zero). The initial (ground) state distribution (panel (a)) has two maxima along Z = 0, which correspond to the dominant covalent nature of the ground state wavefunction. At the maximum of the field, the distribution has changed significantly. It is moved in the positive Z direction. For the sake of comparison, the dotted white circles display the location of the maximum in the ground state probability distribution. Now a significant part of the distributions is found at z = 0 and Z = 1 a.u., which corresponds to the localization of both electrons at one of the two nuclei (i.e. that one in positive Z direction). At the next zero of the field, the probability distribution is relaxed back to the original covalent state distribution. Thus, these results clearly demonstrate a correlated two-electron dynamics in the hydrogen molecule, as predicted by other authors before [30].

Single ionization of the hydrogen molecule proceeds predominantly via the ionic H^+–H^- state, which is strongly populated at the maxima of the field. This can be seen when the snapshot of the Z—z distribution, taken at the field maximum (Fig. 4b), is presented on a logarithmic scale, as displayed in Fig. 5. The two dashed white lines represent the expected directions of single ionization from the covalent and the ionic part of the wave packet. One clearly sees from these results that ionization from the ionic state dominates, in agreement with the earlier theoretical results [29, 30].

3.2. Mechanisms of Nonsequential Double Ionization

Figures 6 to 9 show a series of snapshots of the evolution of the two-electron probability distribution during the laser pulse. They reveal the dynamics leading to the emission of both electrons in the field. Panel 6a and those panels in the left column of each Figure show the distribution in the Z–z space, integrated over the ρ coordinate. The bound state population is located in the middle of the plots, the single ionized population is concentrated near the z_1 and the z_2 axes, which are located along the diagonals in the Z–z plots, and the double ionized population is found in the regions in between these axes (c.f. Fig. 2). The plots in Fig. 6b and in the right-hand columns of Figs. 7–9 offer the complementary view on the distributions in the Z–ρ plane, integrated over the z coordinate. Distribution located in these plots at small ρ indicate electron dynamics along the polarization axis, while parts at large ρ correspond to an off-axis motion of the electrons.

The snapshots in Fig. 6 correspond to an instant of time (t = 166 a.u.) after the first major maximum of the field. As expected, these panels show the emission of a singly ionized electron wavepacket along the z_1 and the z_2 axes in the positive Z direction. The population occurs at small ρ, indicating a propagation along the polarization axis. This is on the one hand a consequence of the 1D approximation of the center-of-mass motion along the polarization direction in our model. Since in single ionization the second electron remains

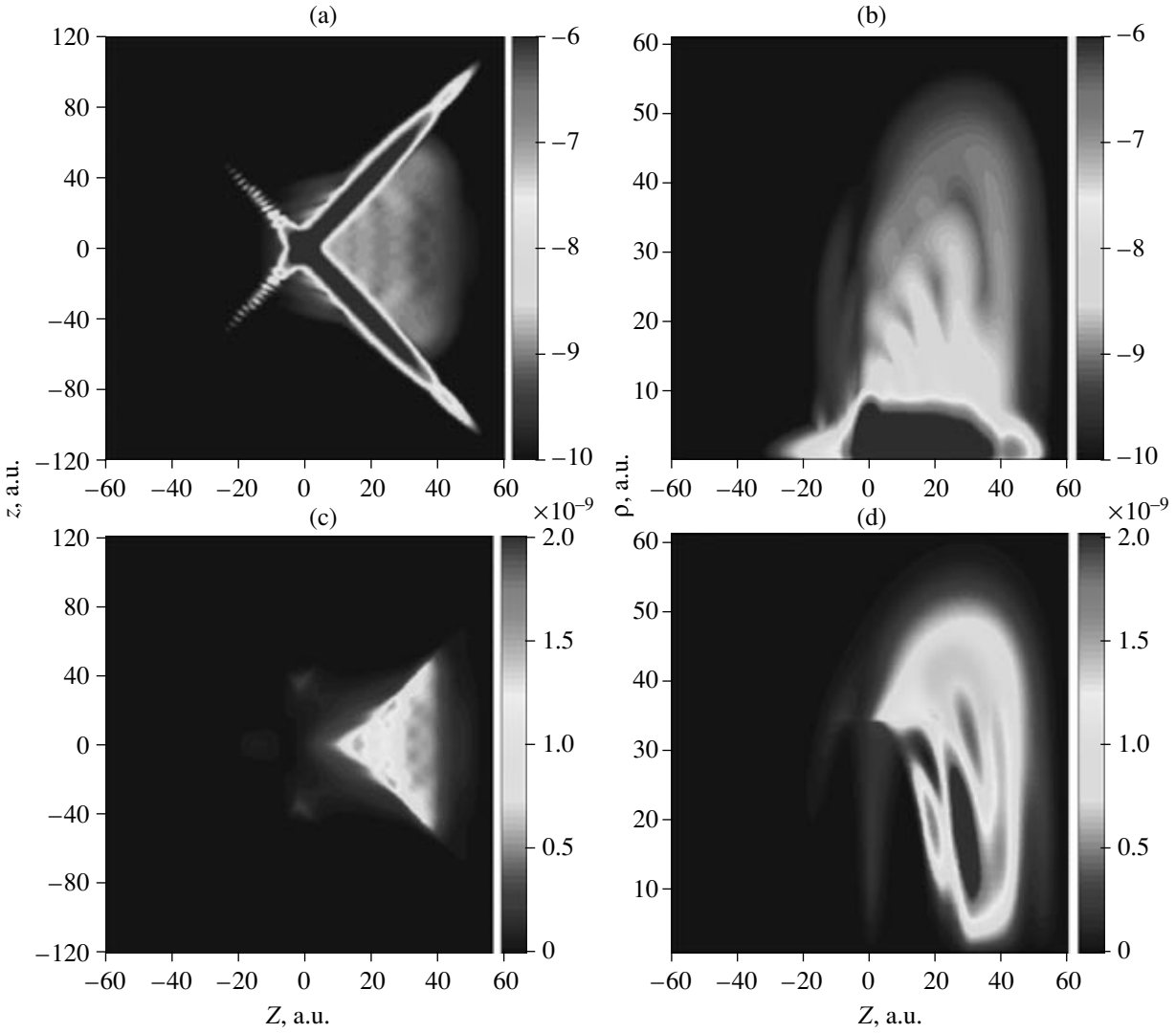

Fig. 7. Probability distributions integrated over (a, c) ρ, and (b, d) z at t = 175 a.u. The panels in the upper row display the whole density while those in the lower row show the part of distribution located in the doubly ionized region only.

bound near the nuclei (i.e., it is confined to small ρ), the ionized electron wave packet will have to propagate along the polarization axis. On the other hand, this is in agreement with many previous experimental and theoretical observations that single ionization appears predominantly along the polarization axis.

Next, we turn to the distributions at t = 175 a.u., i.e., shortly after the zero of the field in the middle of the pulse, shown in Fig. 7. From the panels in the upper row of the figure, one clearly sees a strong double ionization dynamics in both the Z–z and the Z–ρ distributions. This becomes particularly obvious from the plots in the lower row, in which only the doubly ionized distribution (probability density) is shown (c.f. Fig. 2). The doubly ionized wave packet mainly occurs in the right triangle of the double ionization region in the Z–z distribution (left hand columns), which corresponds to an emission of both electrons to the same side of the nuclei with respect to the polarization axis. This result is in agreement with the recollision picture [13]: A singly ionized wavepacket, which has been emitted near the field maximum at t = 88 a.u., has been first accelerated by the field in negative Z direction, before it is driven back to the ion and rescatters with the ion near the zero of the field (t = 151 a.u.), leading to the joint escape of both electrons to the same side of the nuclei. Due to the interelectron repulsion, the electrons experience a strong transversal dynamics, as can be seen from the Z–ρ distributions on the right hand side of the Fig. 7, which is in agreement with experimental observations [31] and S-matrix calculations [32].

In the snapshots, taken shortly after the next field maximum at t = 201 a.u. (c.f. Fig. 8), a second pathway to double ionization of the hydrogen molecule becomes apparent. The Z–z distribution shows elongated structures in the upper and lower triangle of the double ion-

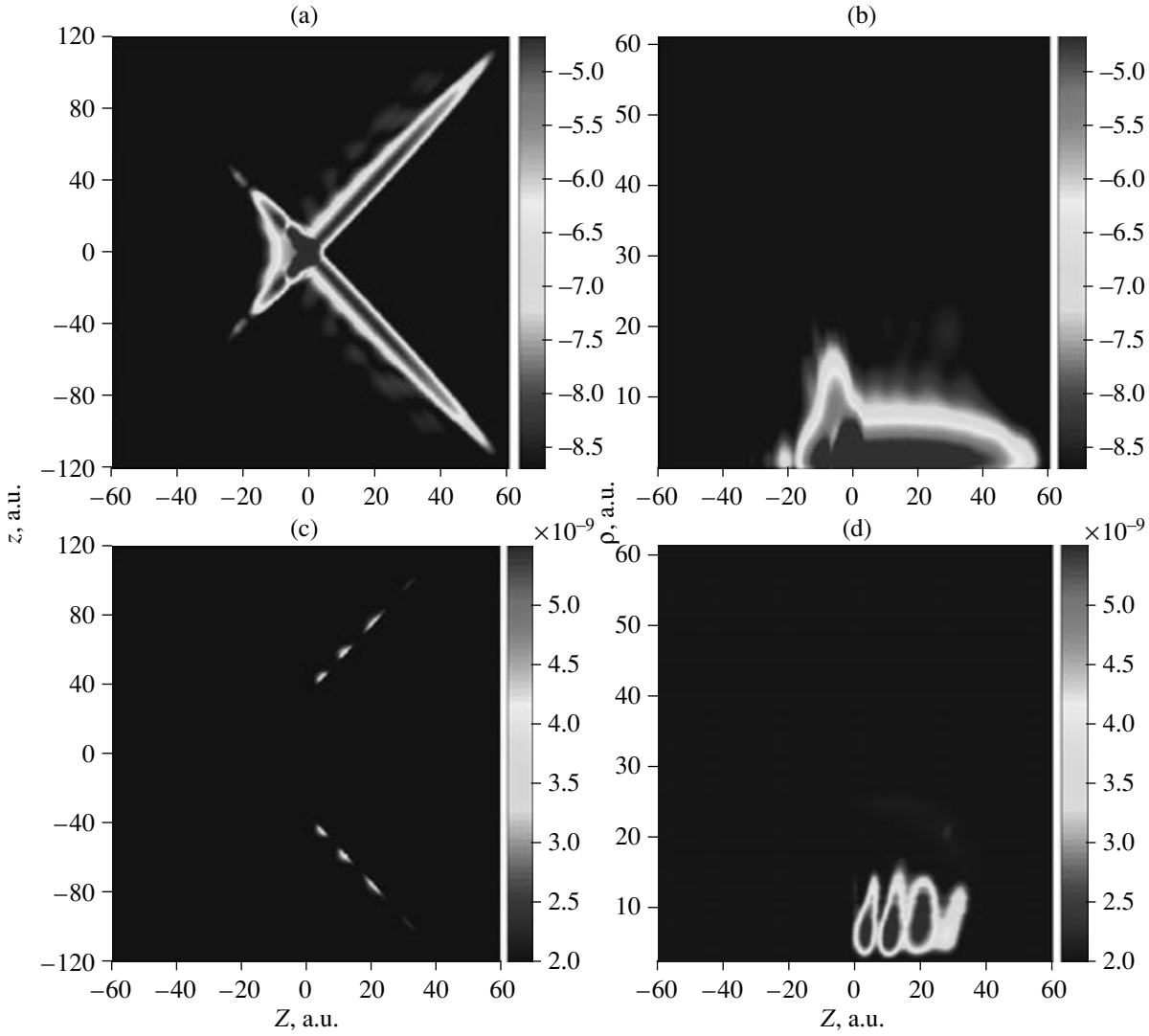

Fig. 8. Same as Fig. 7 but at t = 201 a.u.

ization region, which are detached parallel to the z_1 and z_2 axes. Thus, both electrons are ejected to opposite sides of the nuclei and the correlation between them is small, as the confinement of the probability distribution at low ρ shows (right-hand panels). This contribution corresponds to the small rise in the double ionization probability (c.f. Fig. 3) and, as outlined above, is due to field ionization from excited states of the H_2^+ molecule. The excitation of the ion is found [23] to arise most likely due to rescattering of the electron wave packet at the previous field zero. Thus, this contribution is indeed a second pathway to nonsequential double ionization, as has been proposed before by an empirical analysis of experimental data [21].

It is expected that the double ionization scenarios analyzed above repeat every half cycle. This includes recollision of a previously single ionized electron wave packet at a field zero causing a direct transition of the second electron to the continuum or an excitation of the ion, followed by field ionization of the excited states at the next maximum of the field amplitude. This agrees with the results of our numerical calculations, as can be seen from the snapshots at later instants of time, presented in Fig. 9. At t = 230 a.u. (zero-crossing of the field, panels in upper row) there is again a joint emission of both electrons to the same side of the nuclei. As before (c.f. Fig. 7), this contribution arises due to direct double ionization upon rescattering of a single ionized electron wave packet. Since the field changes sign every half cycle of the pulse, the two electrons are emitted in the –Z direction, i.e., in the opposite direction as the contribution shown and discussed in Fig. 7. As in Fig. 7, there is seen a strong dynamics in the double ionization distribution perpendicular to the polarization axis due to the electron-electron repulsion. Finally, the second pathway to double ionization, namely, via field ionization of excited states, manifests itself again at t =

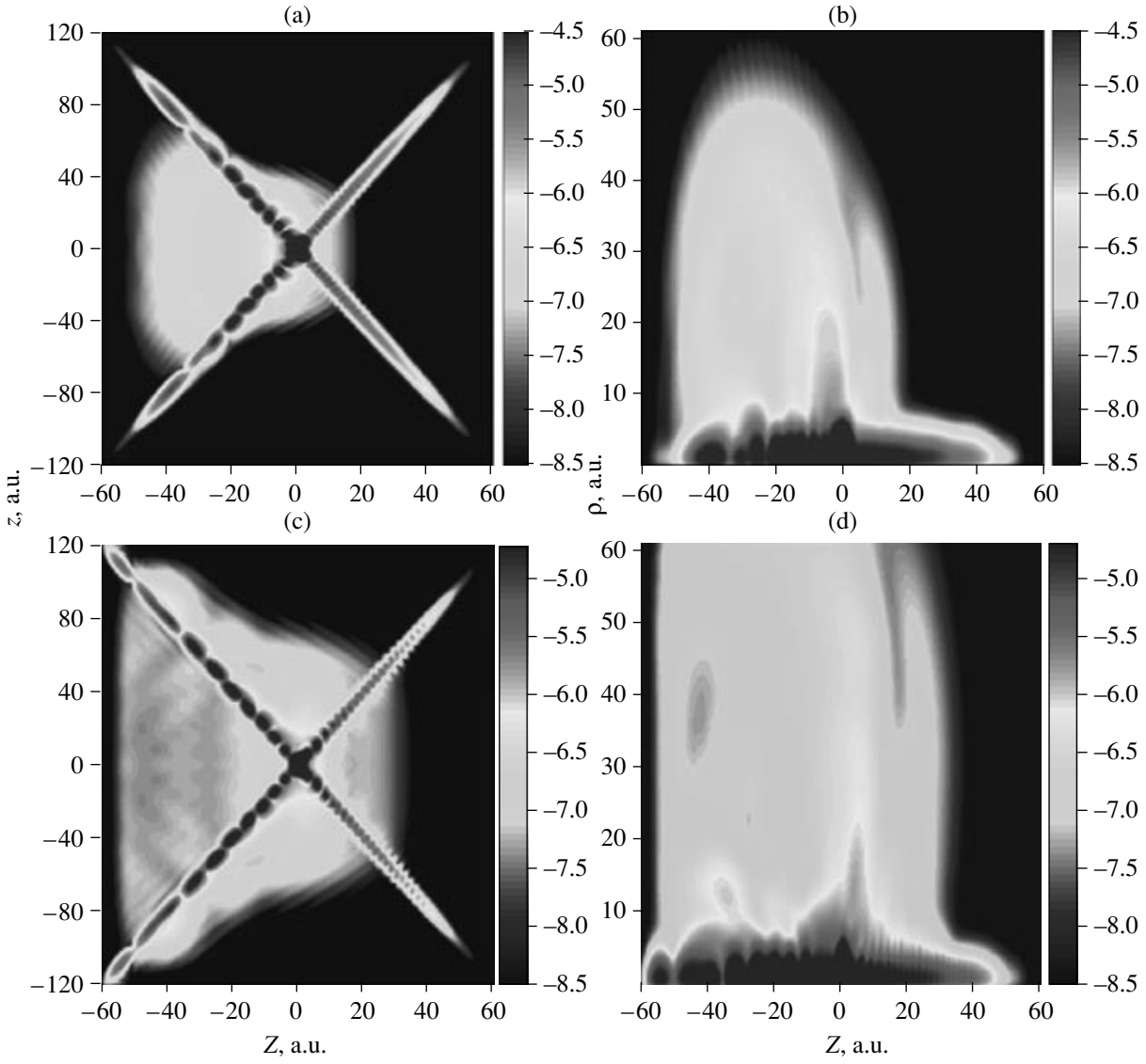

Fig. 9. Probability density integrated over (a, c) ρ, (b, d) z at (a, b) t = 230 a.u. and (c), (d) at t = 252 a.u.

252 a.u. (field maximum; plots in the lower row of Fig. 9). Since the amplitude of the field at t = 252 a.u. is much smaller than that at the previous main maximum, the contribution found in the upper and lower triangles of the double ionization region is smaller in strength as compared to the previous contributions.

3.3. Rescattering Effects

As discussed above, our results allow us to identify and characterize two mechanisms leading to double ionization. Are they however really linked to the return of the previously single ionized electron wave packet to the residual ion, as discussed above? This was able to be shown [23] in test calculations, where we have used additional absorbing boundaries to inhibit the return of parts of the single ionized wave packet. The results show that the double ionization contributions, seen in the previous figures, are partially or totally suppressed as soon as the additional absorbers are used. Moreover, it is possible to interpret the interference structures, which are found in the double ionization probability distributions (c.f., e.g., Figs. 8 or 9), as arise due to the interference of the contributions corresponding to the short and long quantum paths of the electron wave packet.

In Fig. 10, these results are exemplified by a comparison between Z–z distributions at t = 221 a.u., obtained on the full grid (panel (a)) and on a small grid (panel (b)), with Z = (–8…8) a.u. and z = (–16…16) a.u.). In the latter calculations, almost the whole single ionized electron wave packet is absorbed at the boundaries before it returns to the residual ion, i.e., the rescattering scenario is suppressed. The comparison of the results

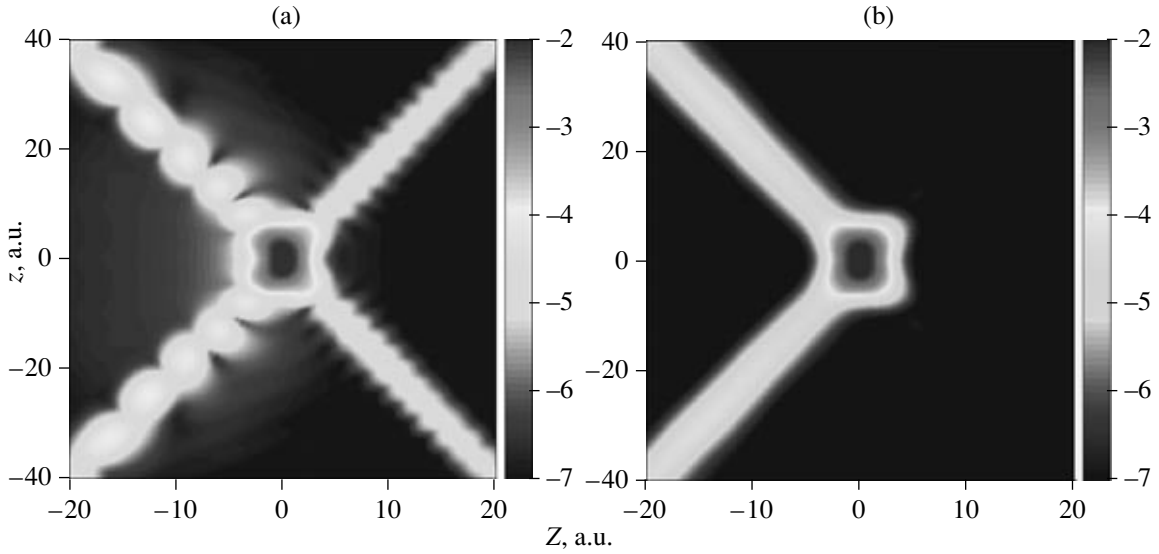

Fig. 10. Probability density integrated over ρ at $t = 221$ a.u. (a) on a smaller grid ($Z = (-8\ldots8)$ a.u.; $z = (-16\ldots16)$ a.u.) and (b) the full grid.

shows distinct differences: First, there is almost no double ionization contribution found in the calculation on the small grid. This lets us to conclude that the pathway of joint emission of both electrons to the same side is directly related to the return of the single ionized electron wavepacket. Second, we note that, in the results of the small-grid calculations, interferences in the single ionization region (along the z_1 and z_2 axes in the diagonal) disappear. We interpret these structures (c.f. [12]) as due to the interference between the returning electron wave packet and the newly ionized electron wave packet (see also [33, 34]).

4. CONCLUSIONS

In conclusion, we have presented ab initio model calculations of the two-electron dynamics in H_2 in a strong few-cycle laser pulse beyond the conventional one-dimensional approximation. In the model, the full dynamics of the two electrons in their relative coordinate is preserved, while the center-of-mass motion is restricted to 1D along the polarization direction. The results of our numerical calculations have revealed two-electron effects in the single and double ionization of the hydrogen molecule. It has been confirmed that the formation of ionic H^+H^- states is the doorway state to single ionization of the H_2 molecule. Two pathways to nonsequential double ionization have been identified, namely the emission of a correlated electron pair at the zeros of the field, which shows a strong transversal dynamics, and the electron emission from previously excited ionic states of the molecular ion near the maxima of the field. It is shown that both mechanisms are linked to the return of the single ionized wave electron wave packet to the ion.

ACKNOWLEDGMENTS

We thank H. Kono and L. Roso for stimulating discussions. We acknowledge partial support from DAAD (project no. D/05/25690), MEG (HA2005-0158), GGI-MEC (FIS2005-01351) and NSERC Canada (SRO grant no. 5796-299409/03).

REFERENCES

1. J. H. Posthumus, Rep. Prog. Phys. **67**, 623 (2004).
2. P. H. Bucksbaum, A. Zavriyev, H. G. Muller, and D. W. Schumacher, Phys. Rev. Lett. **64**, 1883 (1990).
3. L. J. Frasinski, J. H. Posthumus, J. Plumridge, et al., Phys. Rev. Lett. **83**, 3625 (1999).
4. J. H. Posthumus, J. Plumridge, J. Frasinski, et al., J. Phys. B: At. Mol. Opt. Phys. **33**, L563 (2000).
5. K. Codling, L. J. Frasinski, and P. A. Hatherly, J. Phys. B: At. Mol. Opt. Phys. **22**, L321 (1989).
6. T. Zuo and A. D. Bandrauk, Phys. Rev. A **52**, R2511 (1995).
7. T. Seideman, M. Yu. Ivanov, and P. B. Corkum, Phys. Rev. Lett. **75**, 2819 (1995).
8. F. Légaré, I. V. Litvinyuk, P. W. Dooley, et al., Phys. Rev. Lett. **91**, 093002 (2003).
9. A. S. Alnaser, X.-M. Tong, T. Osipov, et al., Phys. Rev. Lett. **93**, 183202 (2004).
10. A. Staudte, C. L. Cocke, M. H. Prior, et al., Phys. Rev. A **65**, 020703 (2002).
11. H. Sakai, J. J. Larsen, I. Wendt-Larsen, et al., Phys. Rev. A **67**, 063404 (2003).
12. C. Ruiz, L. Plaja, L. Roso, and A. Becker, Phys. Rev. Lett. **96**, 053001 (2006).
13. P. B. Corkum, Phys. Rev. Lett. **71**, 1994 (1993).
14. M. Y. Kuchiev, Pis'ma Zh. Eksp. Teor. Fiz. **45**, 319 (1987) [JETP Lett. **45**, 404 (1987)].

15. M. Y. Kuchiev, JETP Lett. **45**, 404 (1987).
16. K. J. Schafer, B. Yang, L. F. DiMauro, and K. C. Kulander, Phys. Rev. Lett. **70**, 1599 (1993).
17. M. Y. Kuchiev, J. Phys. B: At. Mol. Opt. Phys. **28**, 5093 (1995).
18. A. Becker and F. H. M. Faisal, J. Phys. B: At. Mol. Opt. Phys. **29**, L197 (1996).
19. A. Becker and F. H. M. Faisal, Phys. Rev. Lett. **84**, 3546 (2000).
20. R. Kopold, W. Becker, H. Rottke, and W. Sandner, Phys. Rev. Lett. **85**, 3781 (2000).
21. B. Feuerstein, R. Moshammer, D. Fischer, et al., Phys. Rev. Lett. **87**, 043003 (2001).
22. E. Eremina, X. Liu, H. Rottke, et al., Phys. Rev. Lett. **92**, 173001 (2004).
23. S. Baier, C. Ruiz, L. Plaja, and A. Becker, Phys. Rev. A **74**, 033405 (2006).
24. A. D. Bandrauk and H. Lu, Phys. Rev. A **72**, 023408 (2005).
25. M. Lein, E. K. U. Gross, and V. Engel, Phys. Rev. Lett. **85**, 4707 (2000).
26. J. Javanainen, J. H. Eberly, and Q. Su, Phys. Rev. A **38**, 3430 (1988).
27. C. Beylerian, S. Saugout, and C. Cornaggia, J. Phys. B: At. Mol. Opt. Phys. **39**, L105 (2006).
28. S. Saugout and C. Cornaggia, Phys. Rev. A **73**, 041406(R) (2006).
29. A. Saenz, Phys. Rev. A **61**, 051402 (2000).
30. I. Kawata, H. Kono, Y. Fujimura, and A. D. Bandrauk, J. Phys. B: At. Mol. Opt. Phys. **38**, S753 (2000).
31. M. Weckenbrock, D. Zeidler, A. Staudte, et al., Phys. Rev. Lett. **92**, 213002 (2004).
32. M. Weckenbrock, A. Becker. A. Staudte, et al., Phys. Rev. Lett. **91**, 123004 (2003).
33. D. G. Arbó, S. Yoshida, E. Persson, et al., Phys. Rev. Lett. **96**, 143 003 (2006).
34. D. Bauer, Phys. Rev. Lett. **94**, 113001 (2005).